

Hypersonic flow over a wedge in the detached shock range

H. G. HORNING

Graduate Aerospace Laboratories, California Institute of Technology
hans@caltech.edu

Abstract

In a recent publication [5] showed that the shock wave stand-off distance and the drag coefficient of a cone in inviscid hypersonic flow of a perfect gas can be expressed as the product of a function of the inverse normal-shock density ratio ε and a function of a cone-angle parameter η , thus reducing the number of independent parameters from three (Mach number, specific heat ratio and angle) to two. By making a large number of Euler computations, analytic forms of the functions were obtained. In this article the same approach is applied to the symmetrical flow over a wedge. It turns out that the same simplification applies and corresponding analytical forms of the functions are obtained. The functions of ε are compared with newly determined corresponding functions for flow over a circular cylinder.

1. Introduction

One of the most important parameters in hypersonic flow is the inverse normal-shock density ratio, which for a perfect gas is

$$\varepsilon = \frac{\rho_\infty}{\rho_s} = \frac{\gamma - 1 + 2/M_\infty^2}{\gamma + 1}, \quad (1)$$

where ρ is density, γ is the ratio of specific heats, and M is the Mach number. The subscripts ∞ and s refer to the free stream and to the immediate post-normal-shock condition.

In the flow over a wedge with given free-stream conditions, the shock wave is straight and attached to the wedge tip when the wedge half-angle θ is sufficiently small. As θ is increased a point is reached at which the flow downstream of the wedge is sonic, so that information about the length of the wedge from tip to shoulder can be communicated to the tip. The shock begins to curve, and, at a very slightly larger value of θ , it detaches from the tip. Results of Euler computations are shown for these three conditions in Figure 1. An example of the power of the parameter ε is the approximation given by [3] for the values of θ and the shock angle β at detachment.

$$\beta_d = \arctan \sqrt{\frac{1}{\varepsilon}}, \quad \theta_d = 2\beta_d - \frac{\pi}{2}. \quad (2)$$

Here the subscript d refers to the detachment condition. The exact values of these detachment angles may be determined from

$$\beta_{de} = \arcsin \sqrt{\frac{(\gamma + 1)M_\infty^2/4 - 1 + \sqrt{\gamma + 1} \sqrt{(\gamma + 1)M_\infty^4/16 + 1 + (\gamma - 1)M_\infty^2/2}}{\gamma M_\infty^2}} \quad (3)$$

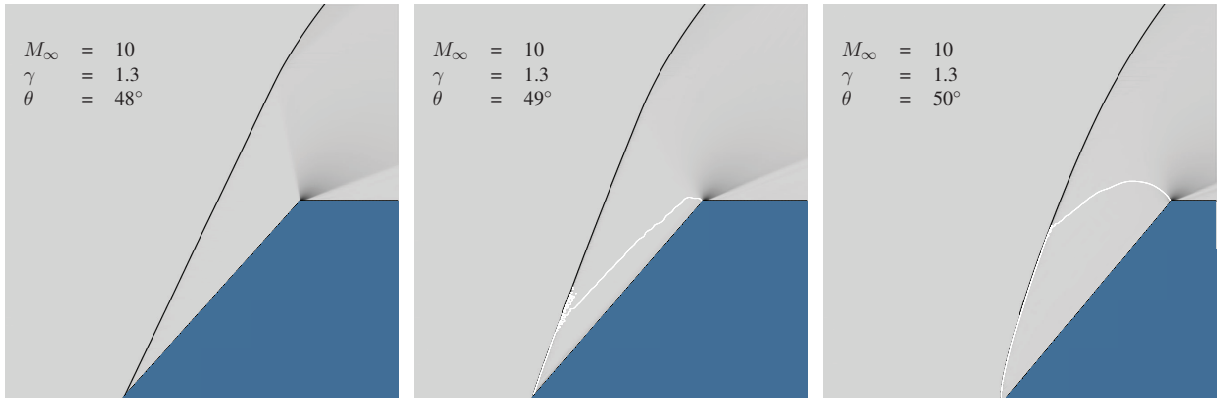


Figure 1: Flow over a wedge at $M_\infty = 10$ and $\gamma = 1.3$ with $\theta = 48, 49$ and 50° , showing (l. to r.) entirely supersonic flow with a straight attached shock, partly subsonic flow with a curved, attached shock and flow with a detached shock. The white line is the sonic line.

$$\theta_{de} = \arctan \left(\frac{(M_\infty^2 \sin^2 \beta_{de} - 1) / \tan \beta_{de}}{1 + [(\gamma + 1)/2 - \sin^2 \beta_{de}] M_\infty^2} \right) \quad (4)$$

Figure 2 shows the quality of the approximation of [3] by plotting exact values for Mach numbers between 4 and 10 and γ between 1.05 and 1.4 together with the approximation vs. ε . As ε increases the approximate value of θ_d falls above the exact curves, especially at the lower Mach numbers.

The range of θ for which the shock is detached is of particular interest here. As in [5], we introduce the variable

$$\eta = \frac{\theta - \theta_d}{\pi/2 - \theta_d}, \quad (5)$$

such that $\eta = 0$ at detachment and $\eta = 1$ at $\theta = \pi/2$. Since analytical formulas for the exact detachment angles exists in the case of wedge flow, we use the variable

$$\eta_e = \frac{\theta - \theta_{de}}{\pi/2 - \theta_{de}} \quad (6)$$

in place of η .

For the shock stand-off distance, Δ , which is of special interest, we again make the hypothesis that it follows the functional form

$$\frac{\Delta}{H} = g(\varepsilon)f(\eta_e) \quad (7)$$

as in [5]. Here H is the height of the wedge measured from the symmetry plane to the shoulder. In order to test the hypothesis, we make a large number of computations covering the parameter space $(M_\infty, \gamma, \theta)$. If the hypothesis is true in the case of flow over a wedge as it was for cone flow, the results can be used to determine the functional forms of g and f .

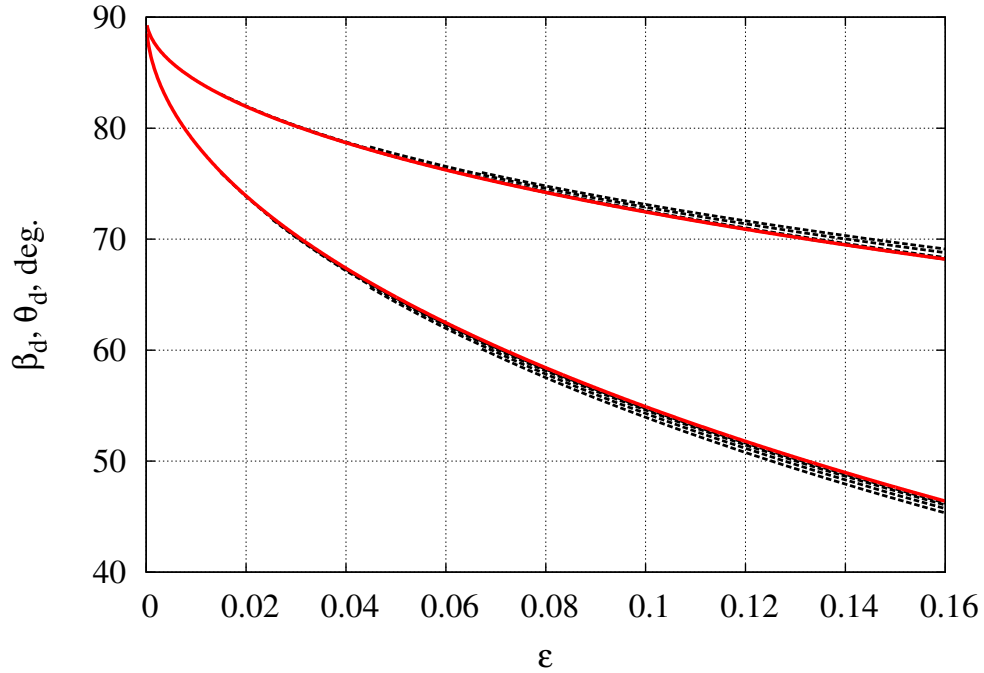


Figure 2: Exact detachment angles for $4 < M_\infty < 10$ and $1.05 < \gamma < 1.4$, plotted with black dashed lines, compared with the approximation of [3] (equations 3 and 4) in red.

2. Discussion of results of computations

2.1. Shock stand-off distance

The parameter space was explored by computing the flow over wedges using the Euler equations. Details about the computational technique are given in the Appendix. An example of the results is presented in Figure 3 for the case of $M_\infty = 5$. Similar results were also obtained for $M_\infty = 4, 7$ and 10 . Plotting the dimensionless shock stand-off distance against ε in the case $\theta = 90^\circ$, (square slab), i. e., for $\eta_e = 1$, where $f(\eta_e) = f(1)$ is a constant, provides a partial test of the hypothesis for the function $g(\varepsilon)$.

This has been done in Figure 4. A fit to the points in Figure 4 yields the interesting result that all points fall on a unique curve given by

$$g(\varepsilon) = \sqrt{\varepsilon} \left(1 + \frac{3}{2} \varepsilon \right), \quad (8)$$

thus confirming the first part of the hypothesis, i. e., that a unique function $g(\varepsilon)$ exists. Again, as in the case of flow over cones, the leading term is proportional to $\sqrt{\varepsilon}$ and the fact that all the results fall on the same curve confirms the first part of the hypothesis. It is interesting that in the corresponding function of ε for the 90° cone, the factor $3/2$ that appears in equation 8 is $1/2$.

To test the second part, four plots of $f(\eta_e) = \Delta/[H g(\varepsilon)]$ vs. η_e are shown in Figure 5 for the four Mach numbers and the four γ 's. All the computational results fall on the same curve given by the unique function

$$f(\eta_e) = 2.2 \eta_e - 0.3 \eta_e^2, \quad (9)$$

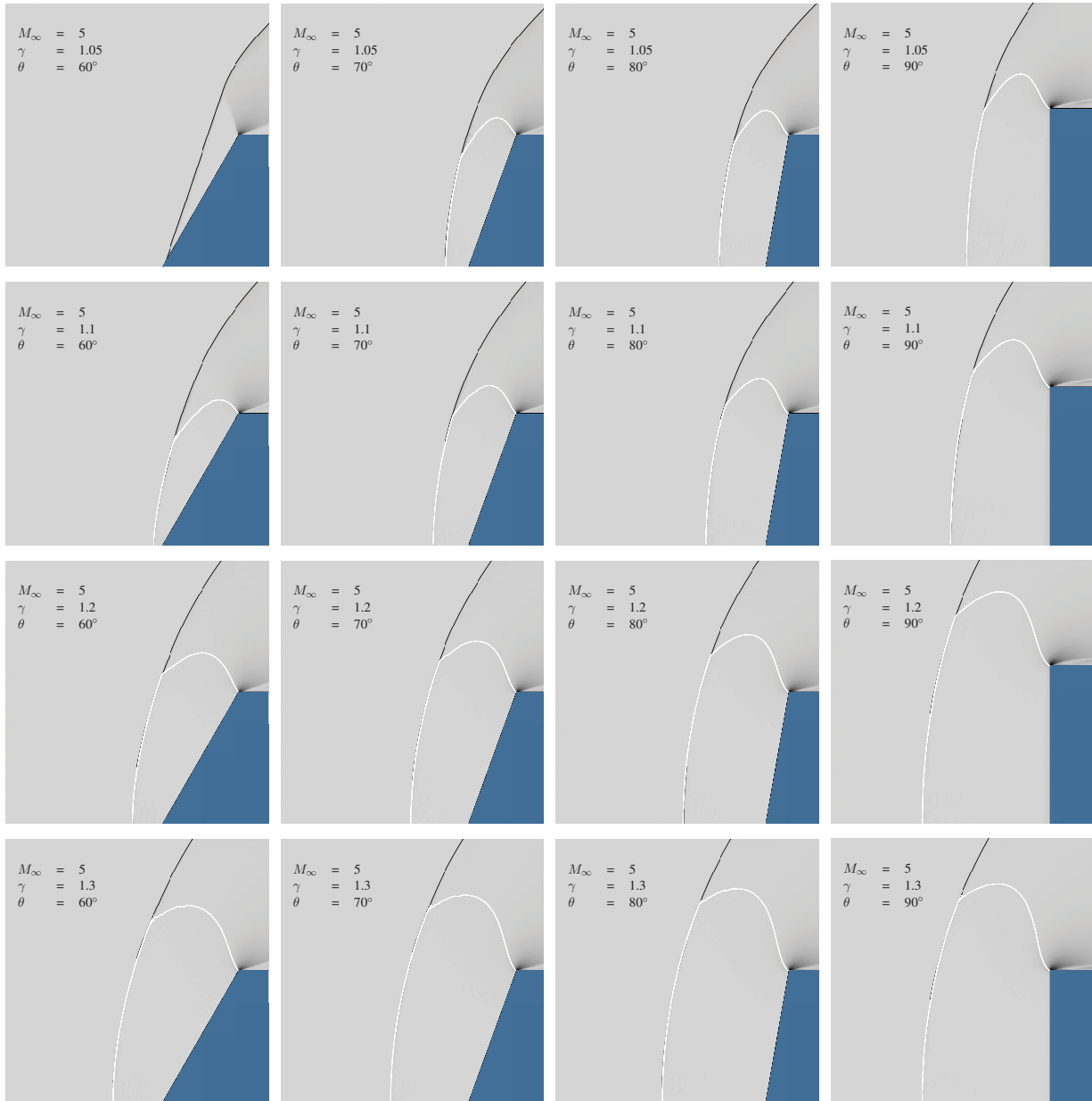


Figure 3: Pseudo-schlieren images of flow over a wedge at $M_\infty = 5$. The grey-shading in these images is proportional to a monotonic function of the magnitude of the density gradient. The white line is the sonic line. In rows from left to right, $\theta = 60, 70, 80$ and 90 deg. In columns from top to bottom, $\gamma = 1.05, 1.1, 1.2$ and 1.3 . Similar sets of computations were made for $M_\infty = 4, 7$ and 10 .

thus confirming the second part of the hypothesis. Note however, that the fit is not so good at $M_\infty = 4$ as for the others. Had we used η instead of η_e , this deterioration of the fit at the lower Mach numbers would have been slightly larger.

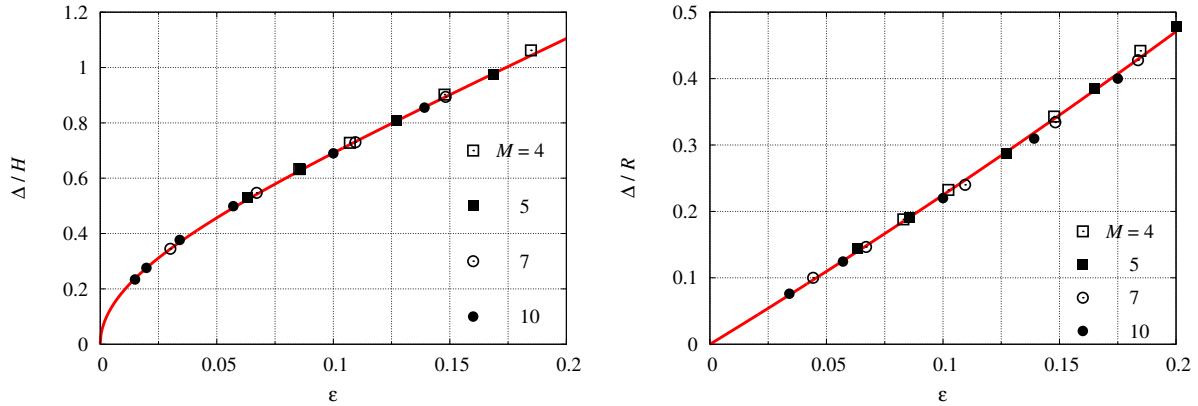


Figure 4: LEFT: Dimensionless shock stand-off distance for flow over a 90° wedge with $M_\infty = 4, 5, 7$ and 10 and $\gamma = 1.05, 1.1, 1.2$ and 1.3 . In the case of $M_\infty = 10$, two cases of $\gamma = 1.01$ and 1.02 , and with $M_\infty = 7$, one case with $\gamma = 1.02$ were added. RIGHT: Corresponding plot for flow over a circular cylinder of radius R . In this case the results are fitted well by $\Delta/R = 2.14\varepsilon(1 + \varepsilon/2)$. In [4] the linear form $\Delta/R = 2.32\varepsilon$ was found, which is only very slightly different.

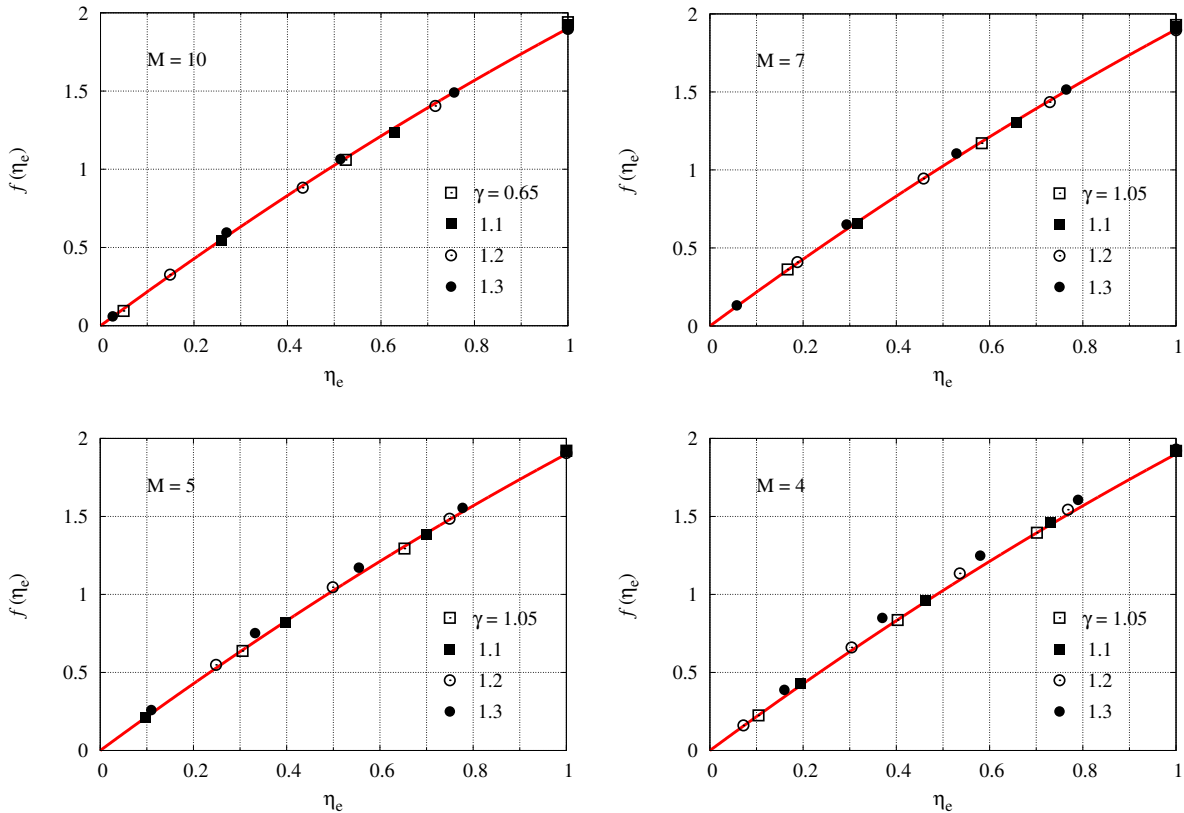


Figure 5: Four plots of $f(\eta_e)$ vs. η_e . Top, left to right: $M_\infty = 10$ and 7 . Bottom, left to right $M_\infty = 5$ and 4 . In all four plots the curve is the same and given by equation 9.

2.2. Drag coefficient

In [5] it was shown that for flow over cones, the drag coefficient could also be expressed in the form of equation 5. Write the drag coefficient for a wedge as

$$C_D = \frac{2D}{\gamma p_\infty M_\infty^2 H L}, \quad (10)$$

where the drag force

$$D = 2L \int_0^H (p - p_\infty) dy,$$

L is the transverse length of the wedge, and y is the distance measured from the symmetry plane of the wedge. Then, if the form of equation 5 holds for C_D , expect that

$$C_D = g_1(\varepsilon) f_1(\eta_e). \quad (11)$$

The same set of computational results can now be used to check whether this is correct. Again we use the case $\eta_e = 1$ where $f_1(1)$ is a constant to check if $g_1(\varepsilon)$ is unique. To this end, Figure 6 shows a plot of C_D vs. ε for the 90° wedge and for the circular cylinder. In both cases all the results collapse onto a single line. for the 90° wedge,

$$C_d = g_1(\varepsilon) = 2 - 1.4\varepsilon, \quad (12)$$

and for the circular cylinder

$$C_D = 1.3 - 5(\varepsilon - 0.085)^2. \quad (13)$$

In order to determine the form of the function $f_1(\eta_e)$ Figure 7 shows four plots of $\Delta/[Hg_1(\varepsilon)]$ vs. η_e . While

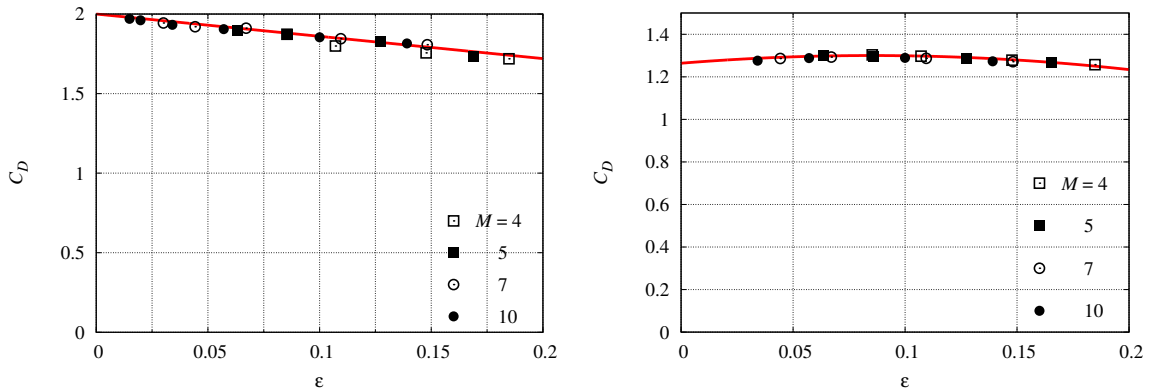


Figure 6: LEFT: Drag coefficient for flow over a 90° wedge with $M_\infty = 4, 5, 7$ and 10 and $\gamma = 1.05, 1.1, 1.2$ and 1.3 . For $M_\infty = 10$, two cases of $\gamma = 1.01$ and 1.02 , and with $M_\infty = 7$, one case with $\gamma = 1.02$ were added. RIGHT: Drag coefficient for flow over a circular cylinder with $M_\infty = 4, 5, 7$ and 10 and $\gamma = 1.05, 1.1, 1.2$ and 1.3 .

the results agree approximately with

$$0.85 + 0.15 \eta_e, \quad (14)$$

they scatter fairly broadly around the line, so that the validity of the functional form is not as convincing as in the case of the shock stand-off distance.

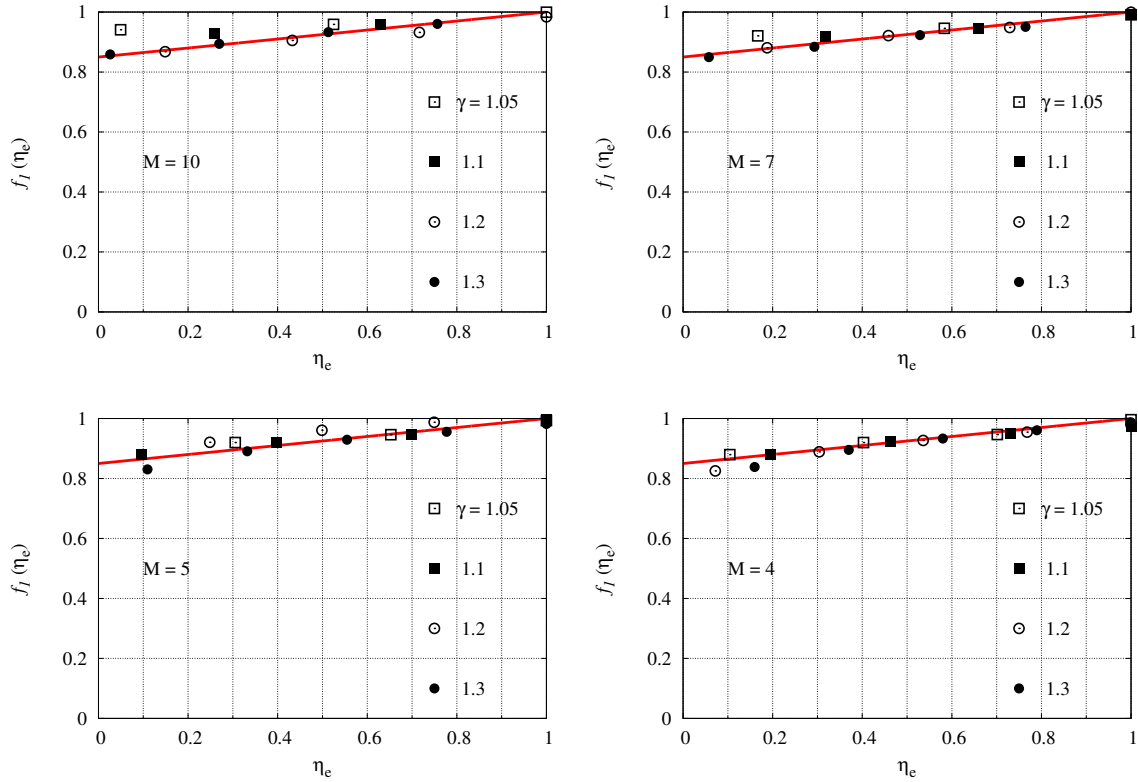


Figure 7: Four plots of $f_1(\eta_e)$ vs. η_e . Top, left to right: $M_\infty = 10$ and 7. Bottom, left to right $M_\infty = 5$ and 4. In all four plots the line is the same and given by equation 14.

3. High-enthalpy effects

Although the results were obtained from perfect-gas computations, they may be expected to apply also to flows at high enthalpy, where vibrational excitation and dissociation may occur and non-equilibrium effects become important. As has been shown by [11] and by [10], forming the density ratio with the average density along the stagnation streamline instead of with the post-normal-shock density causes the results to carry over to the high-enthalpy regime.

4. Conclusions

It was shown that the reduction from three independent parameters to two, in the parameter space defining the dimensionless shock stand-off distance and drag coefficient, that was previously found for axisymmetric hypersonic flow over cones, applies also to flow over wedges in the detached-shock range. Useful analytical forms were found for these relations by performing a large number of Euler computations and plotting the results in the appropriate form. The results are also compared with new results for flow over a circular cylinder.

Acknowledgement

This work was funded by AFOSR FA9550-19-1-0219, PI: J. M. Austin, Contract Officer: I. A. Leyva.

Appendix

The software system Amrita, constructed by James Quirk, see [8], was used. A detailed description of the features and phenomena encountered with some of the algorithms used for Riemann solvers, including the one used here, has also been given by [7]. An example of a test of the software against experiment may be found in [9].

Amrita is a system that automates and packages computational tasks in such a way that the packages can be combined (dynamically linked) according to instructions written in a high-level scripting language. The present application uses features of Amrita that include the automatic construction of the Euler solver, documentation of the code, adaptive mesh refinement according to simply chosen criteria, and scripting-language-driven computation, archiving and post-processing of the results. The automation of the assembly and sequencing of the tasks makes for dramatically reduced possibility of hidden errors. It also makes computational investigations transparent and testable by others. The ability to change one package at a time, without changing the rest of the scheme, facilitates detection of sources of error. In most of the work, the Euler solver generated was an operator-split scheme with HLLC flux (after Harten et al.[2] and Einfeldt [1]) and kappa-MUSCL reconstruction. In some cases with γ close to 1, the carbuncle problem arose, and the more robust equilibrium flux method of [6] was used. The (x, y) plane was discretized by a Cartesian grid of 300×300 coarse-grid cells that are adaptively refined by a factor of 3 to make an effective grid of 900×900 cells. The criterion for adaptation was a chosen threshold of the magnitude of the density gradient. Solid boundaries are represented by a level set defined as the smallest distance of a field point from the solid boundary. The grey-shading of the visualizations is a monotonic function of the magnitude of the density gradient.

References

- [1] B. Einfeldt. On Godunov-type methods for gas dynamics. *SIAM J. Numer. Anal.*, 25:294–328, 1988.
- [2] A. Harten, P. D. Lax, and B. van Leer. On upstream differencing and Godunov-type schemes for hyperbolic conservation laws. *SIAM Rev.*, 25:35–61, 1983.
- [3] W. D. Hayes and R. F. Probstein. *Hypersonic flow theory*. Academic Press, 1959.
- [4] H. G. Hornung. Non-equilibrium flow of nitrogen over spheres and circular cylinders. *J. Fluid Mech.*, 53:149–176, 1972.
- [5] H. G. Hornung, J. Martinez Schramm, and K. Hannemann. Hypersonic flow over spherically blunted cone capsules for atmospheric entry. Part 1, the sharp cone and the sphere. *J. Fluid Mech.*, 871:1097–1116, 2019.
- [6] D. I. Pullin. Direct simulation methods for compressible inviscid ideal-gas flows. *J. Comput. Phys.*, 34:231–240, 1980.
- [7] J. J. Quirk. A contribution to the great Riemann solver debate. *Int. J. for Num. Methods in Fluids*, 18:555–574, 1994.

- [8] J. J. Quirk. Amrita — a computational facility (for CFD modelling). In *VKI CFD Lecture Series*, volume 29. von Karman Institute, 1998.
- [9] J. J. Quirk and S. Karni. On the dynamics of a shock bubble interaction. *J. Fluid Mech.*, 318:129–163, 1996.
- [10] V. P. Stulov. Similarity law for supersonic flow past blunt bodies. *Izv. AN SSSR, Mekhanika Zhidkosti i Gaza*, 4:142–146, 1969.
- [11] C.-Y. Wen and H. G. Hornung. Non-equilibrium dissociating flow over spheres. *J. Fluid Mech.*, 299:389–405, 1995.